Device Characterization of a Sulfur-Implanted p^{++}/p GaSb Photovoltaic Camel Diode

Daniel J. Herrera, *Member, IEEE*, Michael B. Clavel, *Student Member, IEEE*, Mantu K. Hudait, *Senior Member, IEEE*, and Luke F. Lester, *Fellow, IEEE*

***Abstract*—The implantation and rapid thermal annealing of sulfur (S^+) ions has previously been shown to be an effective method in non-epitaxially attaining hole carrier concentrations as high as 1×10^{19} cm^{-3} in gallium antimonide (GaSb). This technique was used to fabricate a photovoltaic diode by delta-doping the front surface of a p-type GaSb substrate and forming a p^{++}/p junction. The steep potential created using this process is increased by strong Fermi level pinning at the metal/p^{++} interface, resulting in a camel diode with a barrier height of 0.51 eV. A post-fabrication etch process succeeded in improving the short circuit current density to 41.8 mA/cm^2 and the internal quantum efficiency to 90% by enhancing the carrier lifetime away from the front metal contact grid. Likewise, the open circuit voltage improved to 0.21 V, with an intrinsic fill factor above 40%. These results offer the potential of a significantly higher power output than similar non-epitaxial devices made on n-type GaSb substrates.**

***Index Terms*—Gallium antimonide (GaSb), ion implantation, non-epitaxial, photovoltaic cells, sulfur doping.**

I. Introduction

GALLIUM antimonide (GaSb) has played a central role in the development of near-infrared (IR) optoelectronic devices, such as thermophotovoltaics (TPV), often as a substrate upon which lattice-matched ternary and quaternary III-V semiconductor layers are epitaxially grown. The low-bandgap PV devices fabricated using these methods [1] have proven to be promising for the development of remote TPV power systems using lower temperature emission sources [2]–[4]. However, in order for near-IR technologies like TPV to become more viable for large-scale production, non-epitaxial device fabrication methods that use the GaSb substrate as the absorbing region must be pursued for their lower production cost [5]. Thus far, the most effective non-epitaxial doping method in GaSb has been the zinc diffusion method [6]–[10], which dopes the surface of an n-GaSb substrate to be heavily p-type, forming a p-n junction. However, this method's reliance on the use of an n-type substrate compromises the device's performance since the collection of photogenerated carriers primarily depends on the diffusion of minority carrier holes, which have a much lower carrier mobility than electrons in GaSb [11]. Additionally, because of the high temperatures used during diffusion, the shape of the diffused doping profile is limited to a surface-centered distribution of approximately Gaussian shape, further imposing limitations on device design.

As an alternative to the diffusion approach, ion implantation has been investigated as a non-epitaxial doping technique. In contrast with diffusion, ion implantation offers higher flexibility with respect to substrate type as well as enhanced control over the depth profile of the doping concentration via the use of multiple implant doses. The possibility of room-temperature processing also enables the use of patterned photoresist as a masking layer, allowing for more sophisticated doping profiles. Nevertheless, implantation has seen relatively little use in the fabrication of GaSb-based devices, typically because of damage and swelling caused by the implants [12]–[15].

Prior research has identified beryllium (Be^+) as a suitable p-type dopant ion in GaSb for moderate carrier concentrations [16]. However, the identification of an n-type dopant in GaSb has been more elusive, with only Group-VI S^+ ions showing some promise. Previous attempts to activate high doses of S^+ ions as substitutional donors [17] have shown that elevated-temperature implantation and long anneal times can only slightly compensate the native hole concentration of an undoped GaSb substrate ($N_h \sim 1 \times 10^{17}$ cm^{-3}) because of sulfur's relatively deep donor level in GaSb [18], [19]. In place of a substitutional implantation, it has recently been shown that implanting GaSb with moderate doses of S^+ ions along with a short anneal time can induce a heavily p-type layer with charge concentrations greater than 1×10^{19} cm^{-3}, while simultaneously repairing the bulk region of the wafer [20].

To demonstrate the flexibility of ion implantation, it would be valuable to investigate the potential of this doping mechanism for the fabrication of a photovoltaic device on a p-type substrate. In this work, the damage-inducing technique is used to form a photovoltaic device consisting of a p^{++}/p junction. The photovoltaic characteristics of this device configuration are reported, and the extrinsic and intrinsic performances are compared. An etch-back of the damaged surface layer is also examined as a means to optimize the device's performance by removing residual damage away from the contacts.

Manuscript received January 10, 2020; revised March 25, 2020 and May 21, 2020; accepted August 5, 2020. Date of publication September 3, 2020; date of current version October 21, 2020. This work was supported in part by the Institute for Critical Technology and Applied Science at Virginia Tech. *(Corresponding author: Daniel J. Herrera.)*

The authors are with the Department of Electrical and Computer Engineering, Virginia Polytechnic Institute and State University, Blacksburg, VA 24061 USA (e-mail: dherrera@vt.edu; mbclavel@vt.edu; mantu@vt.edu; lflester@vt.edu).

Color versions of one or more of the figures in this article are available online at https://ieeexplore.ieee.org.

Digital Object Identifier 10.1109/JPHOTOV.2020.3016615

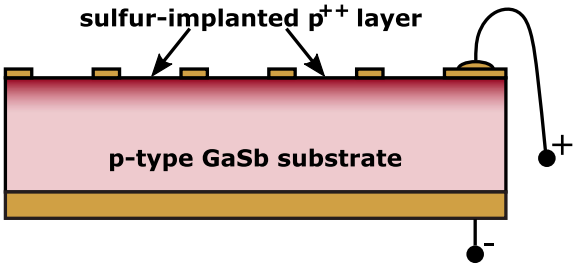

Fig. 1. Device structure of p^{++}/p GaSb photovoltaic formed via a double S^+ ion implantation into an unintentionally doped p-type GaSb substrate and subsequent rapid thermal anneal.

II. Experimental Details

The front surface of an unintentionally doped p-type GaSb substrate ($p = 1.6 \times 10^{17}$ cm^{-3}) was implanted with two separate S^+ ion implant doses of 1×10^{14} and 6.5×10^{13} cm^{-2} at accelerating energies of 190 and 38 keV, respectively. According to secondary-ion mass spectrometry, the depth of the peak ion concentration was found to be 40 nm below the surface, while that of the deeper implant was 177 nm below the surface, with the tail of the latter profile decreasing below the background doping at 400nm [20]. Both sides of the implanted substrate were coated with a protective film of silicon nitride (Si_3N_4) via plasma-enhanced chemical vapor deposition and subsequently annealed at 600° for 10s in a nitrogen ambient. The double implant and anneal procedure used here resulted in a positive surface charge layer with hole concentrations in excess of 1×10^{19} cm^{-3}, with sheet hole concentrations over three times larger than the total implanted dose. This result, along with the inverse correlation between measured hole concentrations and hole mobilities, implies that the p-type concentration was linked to the amount of residual damage, as opposed to a substitutional activation of S^+ ions as donors. Meanwhile, X-ray diffraction crystallography revealed that the anneal process repaired the implant-induced damage in the bulk region such that it was returned to its pre-implant structural condition, suggesting that the positive surface charge is a result of the vertical migration of implant-induced vacancies toward the surface from the bulk. The material and electrical characterization of the implanted material are described in greater detail in a previous work [20].

Fig. 1 shows the cross-sectional structure of the photovoltaic device fabricated on the S^+-implanted GaSb substrate. Prior to device fabrication, the substrate was soaked for 3 min in diluted AZ 400 K developer solution (1:4 in H_2O), which has been shown to etch away the Ga-rich surface layer because of partial Sb diffusion during the anneal procedure [16], [20]. For the front metal, annealed Pd/Ge was used to contact the GaSb surface, along with a thick Au layer for wire-bonding atop a Pt diffusion barrier [21]. The metal stack (Pd/Ge/Au/Pt/Au) was deposited via contact photolithography, e-beam metal evaporation, and liftoff. Immediately before loading into the e-beam vacuum chamber, the native oxide was removed by soaking in a diluted hydrochloric acid (HCl) solution (1:3 in H_2O) for 30 s. The front metal contact grid was arranged in a solar cell comb pattern (2×2 mm area), with metal grid fingers spaced 47.5 μm apart, extending perpendicularly from a central busbar with a circular bond pad. The contact was then annealed at 290° for 30 s under a nitrogen ambient. The contact to the substrate was formed via a blanket metal deposition of Ti/Pt/Au (Ti as bottom metal) on the backside of the wafer. Devices were electrically isolated via a second photolithography step and a mesa etch using a wet etch solution of H_2O:HCl:H_2O_2 (50:50:1 ratio) for $>$ 3 min. No anti-reflection coating (ARC) was deposited on these devices such that the intrinsic performance of the device could be evaluated. The cells were diced and packaged onto thermally conductive integrated circuits [3] by adhering the back metal to a gold contact pad using a conductive silver epoxy, while the front contacts were wire-bonded to separate pads via gold ball bonding. For comparison, a control device was fabricated via an identical fabrication process done on a p-type substrate that had not been implanted.

The cells' illuminated J-V characteristics were measured at room temperature (300 K) using a dual-zone solar simulator spectrally matched to the AM1.5 G solar spectrum up to 2000 nm. During measurement, the copper heatsink of the cells' packaging was held in contact with a gold-plated chuck to minimize device heating. The shadowing losses because of the front metal contact grid (15.2%) were compensated for after each measurement. The external and internal quantum efficiencies (EQE & IQE, respectively) were obtained by comparing the cells' zero-bias responsivity to that of calibrated Si and PbSe standards over the ranges of 280–1000 nm and 1000–2000 nm, respectively. In this case, the front metal shadowing losses were approximated to be the ratio of the metal grid finger width to the spacing between two consecutive fingers (10%). After initial measurements, the area between the front metal contact fingers was incrementally etched by soaking the wire-bonded device into a diluted AZ 400 K developer solution (1:4 in H_2O), followed by acetone and isopropanol rinses and a N_2 blow dry. After each consecutive etch, the resulting depth was measured with a Zygo IR interferometer, followed by additional J-V and EQE measurements. After the final etch step, the dark J-V was measured both at 290 and at 80 K.

III. Results and Discussion

A. Etch-Back Improvement to AM1.5G-Illuminated J-V and EQE

As shown by the solid black line in Fig. 2, the J_{sc} and V_{oc} for the device fabricated in this work were measured to be 14.8 mA/cm^2 and 160 mV, respectively. The relatively low J_{sc} compared with the zinc-diffused device reported in [10] suggests that the carrier lifetime was significantly diminished, likely by the residual damage at the implanted p^{++} surface. Upon etching the surface area between the front metal fingers, improvements were immediately seen for both J_{sc} and V_{oc}, with the former nearly doubling after etching 130 nm. As the etch progressed, both parameters continued to improve until they converged toward their final values of 41.8 mA/cm^2 and 211 mV, respectively. Upon visual inspection, it can be seen that the series and parallel resistances both decreased, which are proportional to the inverse of the slope dV/dI near $V = V_{oc}$ and

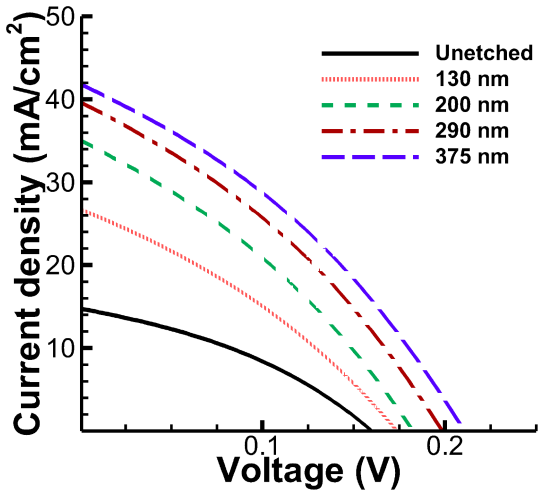

Fig. 2. J-V response of S$^+$-implanted GaSb photovoltaic device in response to an AM1.5 G solar spectrum at 300 K, plotted with respect to the etch depth. Before plotting, the losses because of front metal contact shadowing (15.2%) were compensated for.

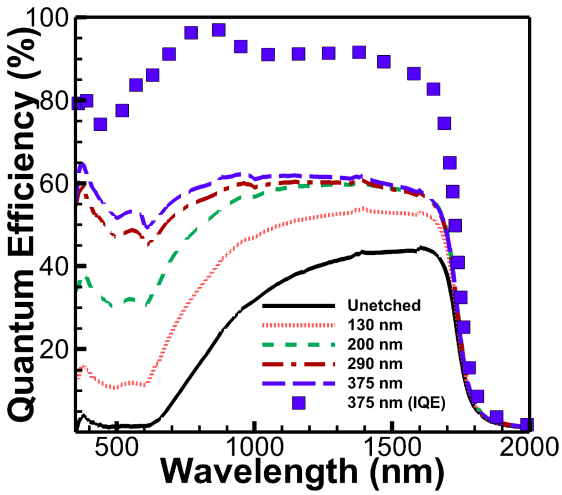

Fig. 3. EQE spectra for S$^+$-implanted GaSb photovoltaic device, before (solid line) and after (dashed lines) progressively wet etching the front surface. Box symbols depict IQE values after the final etching step. Losses because of shadowing (10%) were compensated for before plotting.

$V = 0$, respectively. Etching beyond 350 nm did not continue to improve the performance characteristics and only served to further diminish the parallel resistance. While the final V_{oc} is still comparatively low for a GaSb photovoltaic, the measured J_{sc} above 40 mA/cm^2 is 43%–44% higher than the diffused PV cells reported in [10] and can be attributed to long electron diffusion lengths enabled by the use of the p-type GaSb substrate instead of the more common n-type substrate.

The improvement in the J-V characteristics after etching is also reflected in the EQE, as shown in Fig. 3. Much like the J-V, the measured EQE correspondingly approached a maximum as the depth of the etch increased. The most significant improvement was shown in the visible spectrum, whose efficiency increases from below 5% in the unetched case to above 50% after the final etch step. Meanwhile, the etching procedure increased the near-IR absorption at the cutoff by a factor of 1.5, until it converged near 90%. Since the measured J_{sc} did not eventually decrease to zero after sequential etching and the IQE is greater than 90% for the final etch step, it can be inferred that the photocurrent is governed by the diffusion of photogenerated holes and electrons across the p-type layer. The holes must be collected at the front metal contact and electrons at the back metal contact.

When compared with other works, it is useful to compare the IQE spectra since EQE spectra of GaSb-based devices are often different because of the use of an ARC to maximize the response in a particular spectral region. After the final etch, the measured IQE in the IR region (90%) is roughly equivalent to that of a commercial Zn-diffused device reported in [10]. A similar peak IQE has also been reported by the authors in [22] and [23] for a device with an optimized emitter doping profile. Therefore, it is expected that the etched device in this work would exhibit a similar external IR response with the inclusion of an IR-optimized ARC. For a single-layer Si_3N_4 ARC with a reflectivity of 15% near bandgap, a peak EQE of 75% would be expected for the IR, similar to the commercial device reported in [10].

B. De-Embedding the Effect of Parasitic Resistances From Fill Factor

Despite the significant improvement in both V_{oc} and J_{sc}, the extrinsically measured fill factor (FF$_{ext}$) does not also improve accordingly, ranging between $0.32 \leq \text{FF}_{ext} \leq 0.36$ throughout the etch process. Typically, the fill factor can be estimated directly from the measured V_{oc} [24]; however, it is clear from the J-V characteristics shown in Fig. 2 that the fill factor is being degraded by parasitic resistances, particularly near $V = V_{oc}$. In order to project the full potential of this fabrication technology, the effects of the parasitic series and parallel resistance components (R_s and R_p, respectively) must be de-embedded from the extrinsically measured performance to estimate the intrinsic fill factor (FF$_{int}$).

The fill factor is defined as the ratio of the maximum power point and the $I_{sc}V_{oc}$ product and can be approximated as a function of the open circuit voltage [24]

$$\text{FF} = \frac{v_{m0}^2}{v_{oc}(v_{m0+1})} \tag{1}$$

where v_{oc} is the normalized open circuit voltage defined as $v_{oc} = qV_{oc}/nkT$ and v_{m0} is the normalized voltage at the maximum power point, which can be estimated explicitly in the expression $v_{m0}(v_{oc}) = v_{oc} - ln(v_{oc} + 1)$. The intrinsic open circuit voltage ($V_{oc,int}$) was determined using (1) after extracting the non-ideal R_s and R_p parameters, from which FF$_{int}$ could then be calculated. The effect that these parasitic resistances have on the performance of the device are described by the single-diode model, as shown below

$$I = -I_{ph} + I_0\left(\exp\left(\frac{q(V - IR_s)}{nkT}\right) - 1\right) + \frac{V - IR_s}{R_p}. \tag{2}$$

TABLE I
SELECTED DEVICE PARAMETERS OF THE S^+-IMPLANTED GASB PHOTOVOLTAIC CELL UNDER AM1.5 G ILLUMINATION AT 300 K AS A FUNCTION OF ETCH DEPTH

Etch depth (nm)	$V_{oc,ext}$(mV)	$R_s(\Omega)$	$R_p(\Omega)$	J_0(mA/cm^2)	$V_{oc,int}$(mV)	n	$FF_{ext}(\%)$	$FF_{int}(\%)$
0	160	54.3	806	2.92×10^{-4}	180	1.90	35.7	39.4
130	174	48.1	352	5.47×10^{-4}	207	2.29	32.5	38.0
200	183	38.4	185	2.26×10^{-4}	248	2.39	32.7	42.2
290	199	35.7	233	5.60×10^{-4}	246	2.55	33.3	39.9
375	211	35.4	198	6.01×10^{-4}	274	2.64	34.0	42.2

The unitless ideality factor n was used as a fitting parameter to match the experimentally measured fill factors (FF_{ext}) to those obtained by evaluating (1) with respect to the measured open circuit voltages $V_{oc,ext}$. As shown in Table I, the values for n obtained using this method were found to be greater than 1.9 for all etch depths, indicative of a device dominated by recombination and/or tunneling processes. The observed increase in n could also be influenced by an increased series resistance; therefore, in essence, the n determined here is an upper bound for the possible value. The trend of n increasing with etch depth is likely a byproduct of the reduced R_p, corresponding to an increase in current leakage paths.

After obtaining n, the effect of R_s and R_p can then be de-embedded from (2), allowing for the calculation of FF_{int}. The resistance measured at $V = V_{oc}$ is approximately equal to the series combination of R_s and the diode resistance $R_d = dV/dI_d = nkT/qI_{sc}$, allowing for the extraction of R_s. Meanwhile, at $V = 0$, R_d is negligible such that the resistance measured at this point is simply $dV/dI = R_s + R_p$. Resistance values for R_s and R_p, respectively, can be therefore calculated from

$$R_s = \left.\frac{dV}{dI}\right|_{V=V_{oc}} - \frac{nkT}{qI_{sc}} \tag{3}$$

and

$$R_p = \left.\frac{dV}{dI}\right|_{V=0} - R_s. \tag{4}$$

The photocurrent I_{ph} is obtained by evaluating (2) at $V = V_{oc}$, which differs from the measured I_{sc} only by an additional parasitic V_{oc}/R_p term

$$I_{ph} = I_0\left(\exp\left(\frac{qV_{oc}}{nkT}\right) - 1\right) + \frac{V_{oc}}{R_p}. \tag{5}$$

Therefore, the I_{ph} calculated here can be taken as the predicted I_{sc} in the absence of R_p. This expression can be substituted into (2) to obtain I_0 via the following expression:

$$I_0 = \frac{I_{sc}\left(R_s + R_p\right) - V_{oc}}{R_p\left[\exp\left(qV_{oc}/nkT\right) - \exp\left(qI_{sc}R_s/nkT\right)\right]}. \tag{6}$$

Assuming $(\exp(qV_{oc}/nkT)) \gg 1$, the intrinsic open circuit voltage ($V_{oc,int}$) for an ideal R_p can be obtained algebraically

$$V_{oc,int} = \frac{nkT}{q} ln\left(\frac{I_{ph}}{I_0}\right). \tag{7}$$

The intrinsic fill factor FF_{int} can then be determined by evaluating (1) using the $V_{oc,int}$ value obtained here. The results of the parameter extraction as a function of etch depth are shown in Table I. The high values for R_s were because of the low carrier mobility of the implanted surface region, which improved as this layer was etched away. In contrast, R_p was degraded upon repeated etching because of the lengthening of the sidewalls beneath the front metal contacts. These non-idealities could be mitigated via the use of a self-aligned implant process or surface passivation. The fill factor was primarily degraded by the non-ideal R_p, whose effect counteracted the improvement in FF_{ext} associated with an increasing V_{oc}. As a result, the extrinsic fill factors underestimate FF_{int} by as much as 10%. It was determined from these calculations that for a similar device with an ideal R_p, the open circuit voltages could consequently increase beyond 270 mV, making it more comparable to that of similar zinc-diffused devices [10]. Despite the projected $V_{oc,int}$ still being lower in this case, the associated power loss is compensated by an improved FF_{ext} and the high J_{sc}, with the maximum power density of 4.83 mW/cm^2 being as much as 20% higher than that of the zinc-diffused devices in [10], demonstrating the advantage of using a p-type GaSb substrate.

C. Camel Diode Dark Current Model and Parameters

To corroborate the calculated ideality factors, the device's dark J-V curves were fitted before and after etching using a fitting software which accounts for parasitic resistances [25], [26]. The voltage-dependent ideality factor $n(V)$ is calculated as

$$n(V) = \frac{q}{kT}\frac{\partial V}{\partial(lnJ)}. \tag{8}$$

The curve-fitting results are plotted in Fig. 4, where $n(V)$ was found to be stable at 1.75 over the entire voltage range of interest in the unetched case. After etching 375nm, $n(V)$ was shown to increase to values greater than 2, which is consistent with the trend previously shown in Table I. It is also clear that $n(V)$ became less stable after etching, with the effect of R_s becoming apparent at higher voltages. This increase in R_s is in disagreement with the trend shown in Table I; nevertheless, it must be noted that the resistances shown here are only representative of currents directly beneath the metal contacts, whereas the illuminated case also includes photogenerated current away from the contacts.

As previously stated, the depletion region responsible for the diode-like J-V must exist only beneath the front metal contacts, presumably in the form of a Schottky contact. However, when measuring the unimplanted control device, only ohmic behavior was seen, with the illuminated J-V plot strongly resembling a photoconductor rather than a photovoltaic. Therefore, the S^+ implantation was a required step in achieving the surface conditions necessary for the photovoltaic action seen here. The proposed

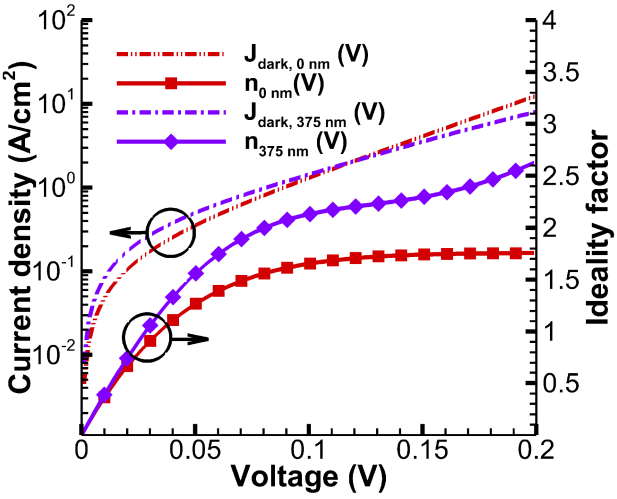

Fig. 4. Dark J-V response (dashed lines, left axis) and ideality factor $n(V)$ (solid lines/symbols, right axis) of S$^+$-implanted GaSb diode at room temperature (300 K) before and after etching 375nm.

band structure for this device is similar to that of a camel diode, in which a delta-doped p^{++} layer is inserted between two intrinsic layers to form a steep triangular potential barrier [27], [28].

A band diagram describing this behavior is given in Fig. 5(a), which shows the valence band maximum at the metal/GaSb interface. Having previously established that the p^{++} characteristic is because of large residual damage at the surface [20], it is assumed that the interface state density is large enough to pin the surface Fermi level to the charge neutrality level of GaSb ϕ_0, which is located 70 meV above the valence band maximum [29], [30]. The resulting p^{++} region is approximated to be a delta-doping layer, whose charge differential with the intrinsic bulk induces a built-in electric field just below the interface [22], [23]. Simultaneously, this degenerately doped layer between the pinned surface and the p-type background doping of the substrate results in a narrow tunneling barrier for holes followed by a triangular potential, whose height is increased by the surface pinning. The diode behavior is because of the accumulation and thermionic emission of holes injected through the tunneling barrier when a positive bias V_F is applied to the front metal. The currents are likely also increased by electrons created via impact ionization, particularly when a reverse bias V_R is applied [31].

To determine the strength of this triangular potential barrier, the reverse saturation current density J_0 was extracted from the dark J-V characteristic. For a camel diode, the calculation for J_0 is identical to that of a Schottky barrier diode [32]

$$J_0 = A^* T^2 \exp\left(\frac{-q\phi_B}{kT}\right) \tag{9}$$

where ϕ_B is the barrier height. The Richardson coefficient A^* was taken to be $4.94A\ \mathrm{cm}^{-2}K^{-1}$ based on the effective mass of electrons in the Γ band for GaSb [33]. The etched device's dark current at 290K was measured and fitted as shown in Fig. 6, from which a reverse saturation current density of $I_0 = 6.0 \times 10\ \mathrm{cm}^{-4}A$ was extracted. At 80 K, the lower ionization

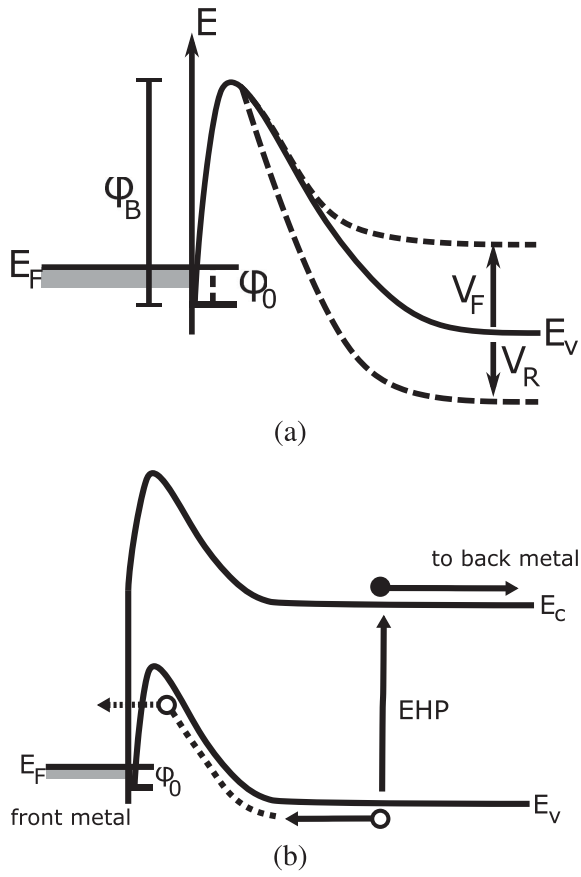

Fig. 5. (a) Band diagram of the metal/p^{++} GaSb interface, where a triangular potential barrier ϕ_B is formed via a strong Fermi level pinning to the charge neutrality level ϕ_0. When a forward bias V_F is applied to the front metal, a hole-dominant dark current is injected from the metal. (b) Extended band diagram showing the extraction of a photogenerated electron–hole pair. Minority electrons are repelled by the camel diode and diffused (solid lines) to the back metal contact. Majority holes diffuse and then drift across the camel diode (dotted line) and subsequently tunnel into the front metal via thermionic field emission.

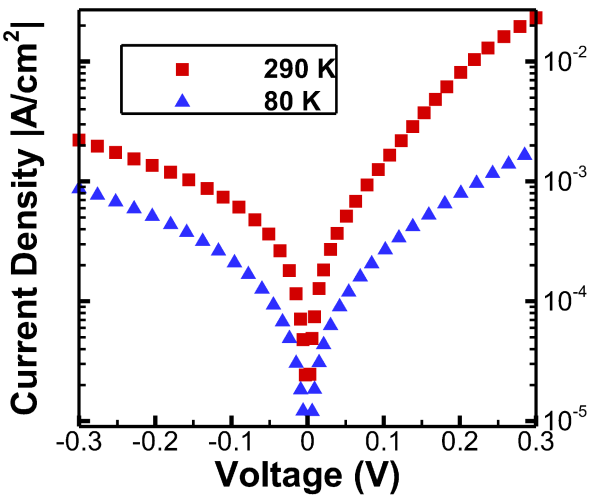

Fig. 6. Dark J-V response of etched S$^+$-implanted GaSb photovoltaic device at 290 and 80 K.

of the implant-induced acceptor states resulted in a reduction of the band bending near the metal/GaSb interface and a nearly ohmic behavior. Using these extracted values, the barrier heights for 290 and 80 K were calculated to be 0.51 and 0.17 eV, respectively. A similar value for the barrier height of 0.16 eV was obtained using Norde's method [34], which calculates ϕ_B for a non-ideal R_s.

IV. Conclusion

The advantages of using a p-type GaSb substrate for a non-epitaxial photovoltaic device were displayed in this work, wherein short circuit current densities above 40 mA/cm^2 were achieved. This result was enabled via a moderately dosed implantation of S^+ ions, whose residual damage caused the surface of a p-GaSb substrate to become extremely p-type. When a front contact metal was deposited on this damaged surface, the combination of the p^{++}/p doping gradient and the surface Fermi level pinning created a steep triangular potential similar to a camel diode. An incremental surface etch process done after metal deposition removed a high recombination surface layer away from the metal contacts, improving the device's IQE to above 90% near bandgap and open circuit voltages near 0.21 eV. A de-embedding of the parasitic resistances revealed that for a more optimized device, the exceptional current densities measured here could lead to higher power outputs than diffused devices made on n-GaSb substrates. This optimized performance could be achieved via a self-aligned implantation and metal deposition process, in which only the area underneath the front metal contacts is implanted via the use of a masking dielectric layer. Furthermore, the optimal device design can be further iterated via the implantation of other small and medium sized ions.

Acknowledgment

The authors would like to acknowledge the Micron Technology Semiconductor Processing Laboratory at Virginia Tech for the use of the cleanroom space.

References

[1] M. W. Dashiell *et al.*, "Quaternary InGaAsSb thermophotovoltaic diodes," *IEEE Trans. Electron Devices*, vol. 53, no. 12, pp. 2879–2891, Dec. 2006.

[2] W. Chan *et al.*, "Modeling low-bandgap thermophotovoltaic diodes for high-efficiency portable power generators," *Solar Energy Mater. Solar Cells*, vol. 94, no. 3, pp. 509–514, 2010.

[3] W. R. Chan *et al.*, "Toward high-energy-density, high-efficiency, and moderate-temperature chip-scale thermophotovoltaics," *Proc. Nat. Acad. Sci.*, vol. 110, no. 14, pp. 5309–5314, 2013.

[4] W. R. Chan *et al.*, "An all-metallic microburner for a millimeter-scale thermophotovoltaic generator," *J. Phys., Conf. Series*, vol. 476, no. 1, 2013, Art. no. 012017.

[5] L. Fraas, J. Avery, and H. Huang, "Thermophotovoltaic furnace–generator for the home using low bandgap GaSb cells," *Semicond. Sci. Technol.*, vol. 18, no. 5, 2003, Art. no. S247.

[6] A. Bett and O. V. Sulima, "GaSb photovoltaic cells for applications in TPV generators," *Semicond. Sci. Technol.*, vol. 18, no. 5, 2003, Art. no. S184.

[7] L. Fraas *et al.*, "GaSb booster cells for over 30% efficient solar-cell stacks," *J. Appl. Phys.*, vol. 66, no. 8, pp. 3866–3870, 1989.

[8] V. Sundaram and P. Gruenbaum, "Zinc diffusion in GaSb," *J. Appl. Phys.*, vol. 73, no. 8, pp. 3787–3789, 1993.

[9] G. Rajagopalan *et al.*, "A simple single-step diffusion and emitter etching process for high-efficiency gallium-antimonide thermophotovoltaic devices," *J. Electron. Mater.*, vol. 32, no. 11, pp. 1317–1321, 2003.

[10] L. Tang, H. Ye, and J. Xu, "A novel zinc diffusion process for the fabrication of high-performance GaSb thermophotovoltaic cells," *Solar Energy Mater. Solar Cells*, vol. 122, pp. 94–98, 2014.

[11] D. Martín and C. Algora, "Temperature-dependent GaSb material parameters for reliable thermophotovoltaic cell modelling," *Semicond. Sci. Technol.*, vol. 19, no. 8, 2004, Art. no. 1040.

[12] A. Milnes *et al.*, "Ion implantation effects in GaSb," *Mater. Sci. Eng., B*, vol. 27, no. 2-3, pp. 129–136, 1994.

[13] R. Callec, P. Favennec, M. Salvi, H. L'Haridon, and M. Gauneau, "Anomalous behavior of ion-implanted GaSb," *Appl. Phys. Lett.*, vol. 59, no. 15, pp. 1872–1874, 1991.

[14] R. Callec and A. Poudoulec, "Characteristics of implantation-induced damage in GaSb," *J. Appl. Phys.*, vol. 73, no. 10, pp. 4831–4835, 1993.

[15] S. Iyer *et al.*, "A study of the ion implantation damage and annealing behavior in GaSb," *J. Electron. Mater.*, vol. 25, no. 1, pp. 119–124, 1996.

[16] N. Rahimi *et al.*, "Beryllium implant activation and damage recovery study in n-type GaSb," in *Proc. SPIE Physics Simul., Photonic Eng. Photovoltaic Devices III*, vol. 8981, International Society for Optics and Photonics, 2014, Art. no. 89811Q.

[17] M. V. Rao *et al.*, "S and Si ion implantation in GaSb grown on GaAs," *J. Appl. Phys.*, vol. 86, no. 11, pp. 6068–6071, 1999.

[18] W. Walukiewicz, "Amphoteric native defects in semiconductors," *Appl. Phys. Lett.*, vol. 54, no. 21, pp. 2094–2096, 1989.

[19] W. Walukiewicz, "Defect reactions at metal-semiconductor and semiconductor-semiconductor interfaces," *MRS Proc.*, vol. 148, pp. 137–148, 1989, doi: 10.1557/PROC-148-137.

[20] D. J. Herrera and L. F. Lester, "Electrical and material characterization of sulfur-implanted GaSb," *J. Vacuum Sci. Technol. B, Nanotechnol. Microelectron., Mater., Process., Meas., Phenom.*, vol. 37, no. 3, 2019, Art. no. 031214.

[21] N. Rahimi *et al.*, "Ultra-low resistance NiGeAu and PdGeAu ohmic contacts on N-GaSb grown on GaAs," in *Proc. IEEE 39th Photovolt. Specialists Conf.*, 2013, pp. 2123–2126.

[22] O. Sulima and A. Bett, "Fabrication and simulation of GaSb thermophotovoltaic cells," *Solar Energy Mater. Solar Cells*, vol. 66, no. 1-4, pp. 533–540, 2001.

[23] G. Stollwerck, O. V. Sulima, and A. W. Bett, "Characterization and simulation of GaSb device-related properties," *IEEE Trans. Electron Devices*, vol. 47, no. 2, pp. 448–457, Feb. 2000.

[24] M. A. Green, "Accurate expressions for solar cell fill factors including series and shunt resistances," *Appl. Phys. Lett.*, vol. 108, no. 8, 2016, Art. no. 081111.

[25] S. Suckow, "2/3-Diode Fit," 2014. [Online]. Available: https://nanohub.org/resources/14300

[26] S. Rißland and O. Breitenstein, "Considering the distributed series resistance in a two-diode model," *Energy Procedia*, vol. 38, pp. 167–175, 2013.

[27] J. Shannon, "A majority-carrier camel diode," *Appl. Phys. Lett.*, vol. 35, no. 1, pp. 63–65, 1979.

[28] K. K. Ng, *Complete Guide to Semiconductor Devices*. New York, NY, USA: IEEE Press, 2002.

[29] J. Tersoff, "Recent models of Schottky barrier formation," *J. Vacuum Sci. Technol. B: Microelectron. Process. Phenom.*, vol. 3, no. 4, pp. 1157–1161, 1985.

[30] W. Walukiewicz, "Mechanism of Schottky barrier formation: The role of amphoteric native defects," *J. Vacuum Sci. Technol. B: Microelectron. Process. Phenom.*, vol. 5, no. 4, pp. 1062–1067, 1989.

[31] Y. Liu, Y. Oyama, P. Płotka, K. Suto, and J. Nishizawa, "Impact ionisation in GaAs planar-doped barrier structures grown by molecular layer epitaxy," *IEE Proc.-Circuits Devices Syst.*, vol. 147, no. 3, pp. 165–170, 2000.

[32] S. M. Sze and K. K. Ng, *Physics of Semiconductor Devices*. Hoboken, NJ, USA: John Wiley & Sons, 2006.

[33] P. Dutta, H. Bhat, and V. Kumar, "The physics and technology of gallium antimonide: An emerging optoelectronic material," *J. Appl. Phys.*, vol. 81, no. 9, pp. 5821–5870, 1997.

[34] H. Norde, "A modified forward I-V plot for Schottky diodes with high series resistance," *J. Appl. Phys.*, vol. 50, no. 7, pp. 5052–5053, 1979.